PCCP

Accepted Manuscript

ROYAL SOCIETY OF CHEMISTRY

www.rsc.org/pccp

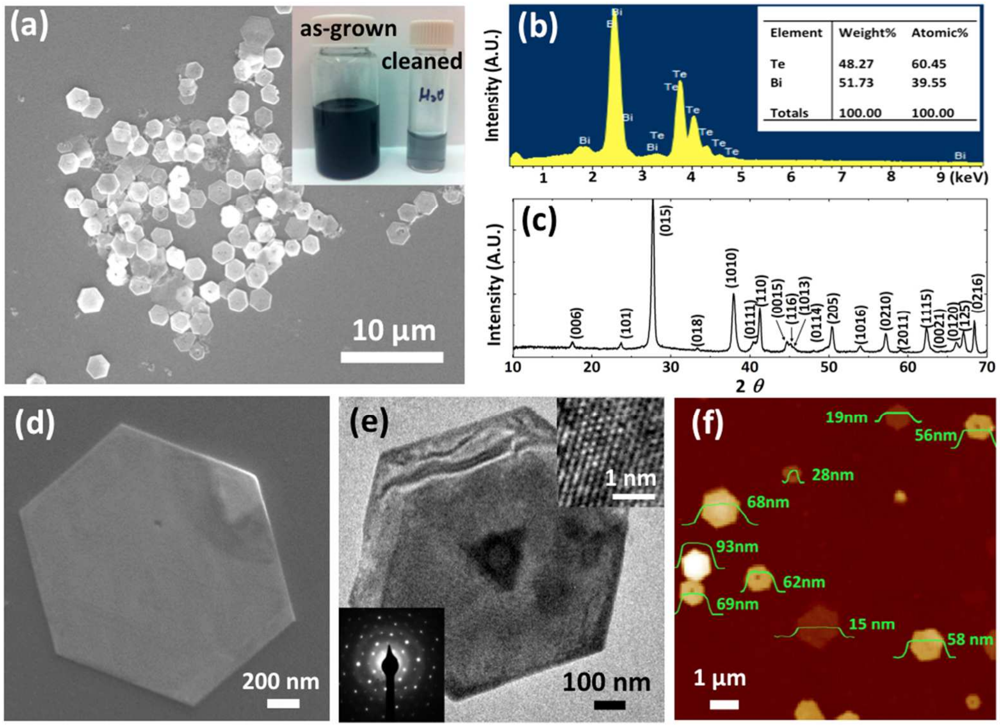

Element	Weight%	Atomic%
Te	48.27	60.45
Bi	51.73	39.55
Totals	100.00	100.00

Figure 1
389x281mm (72 x 72 DPI)

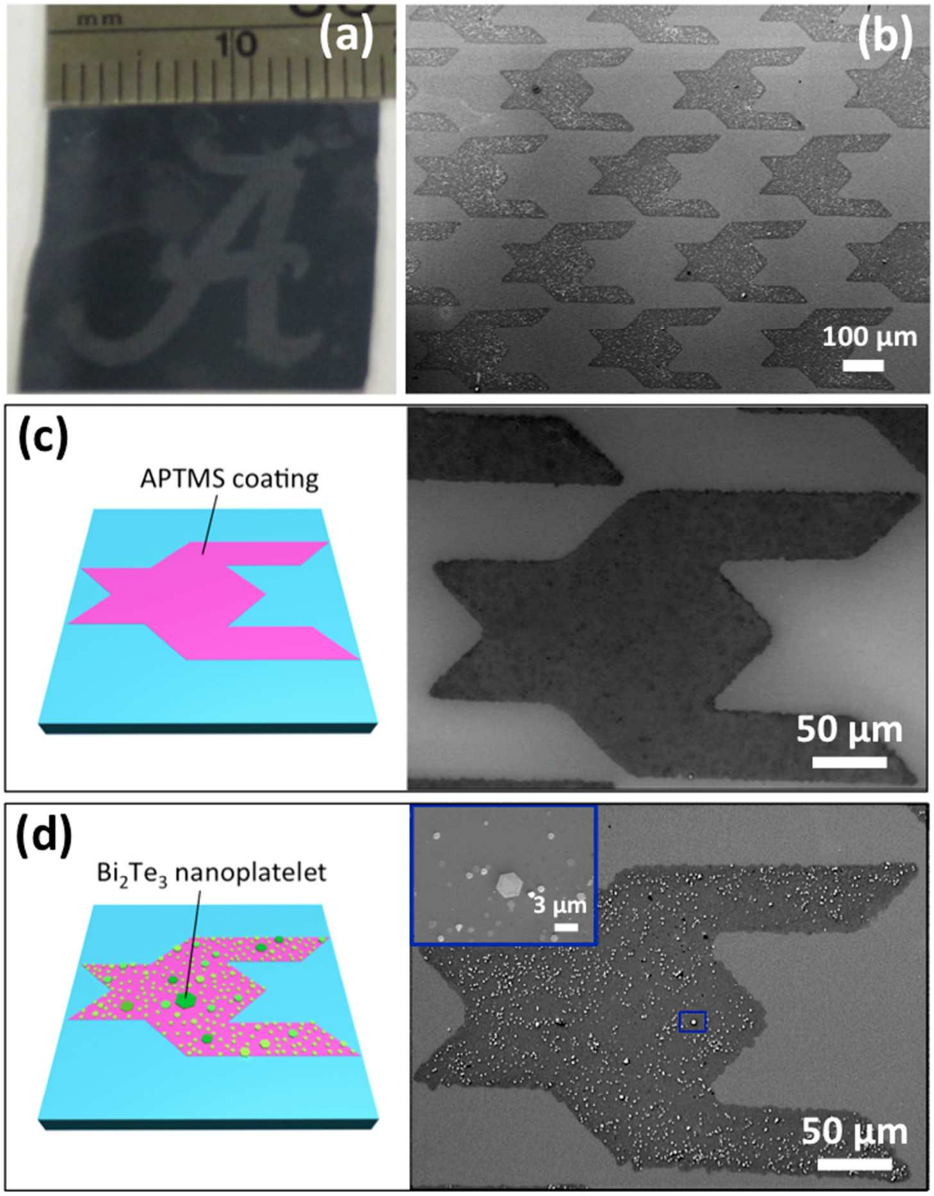

Figure 2
256x328mm (72 x 72 DPI)

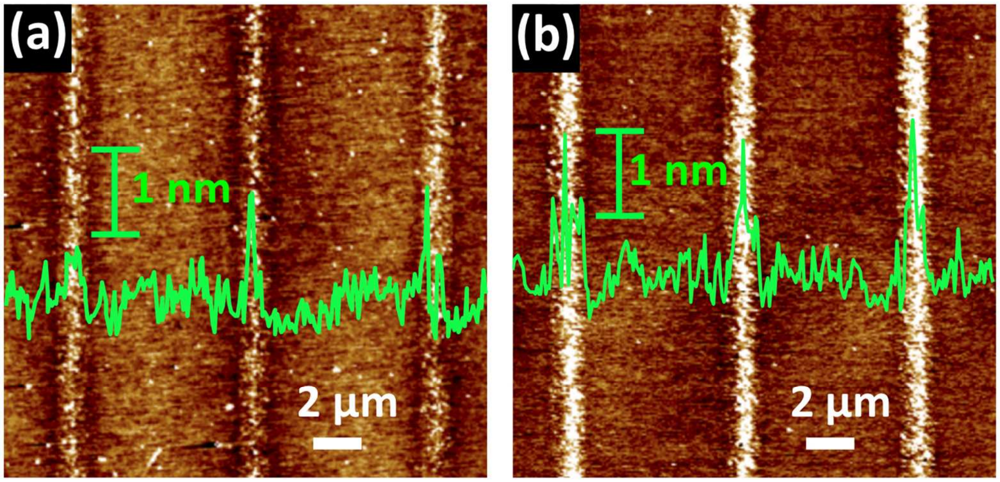

Figure 3
525x252mm (72 x 72 DPI)

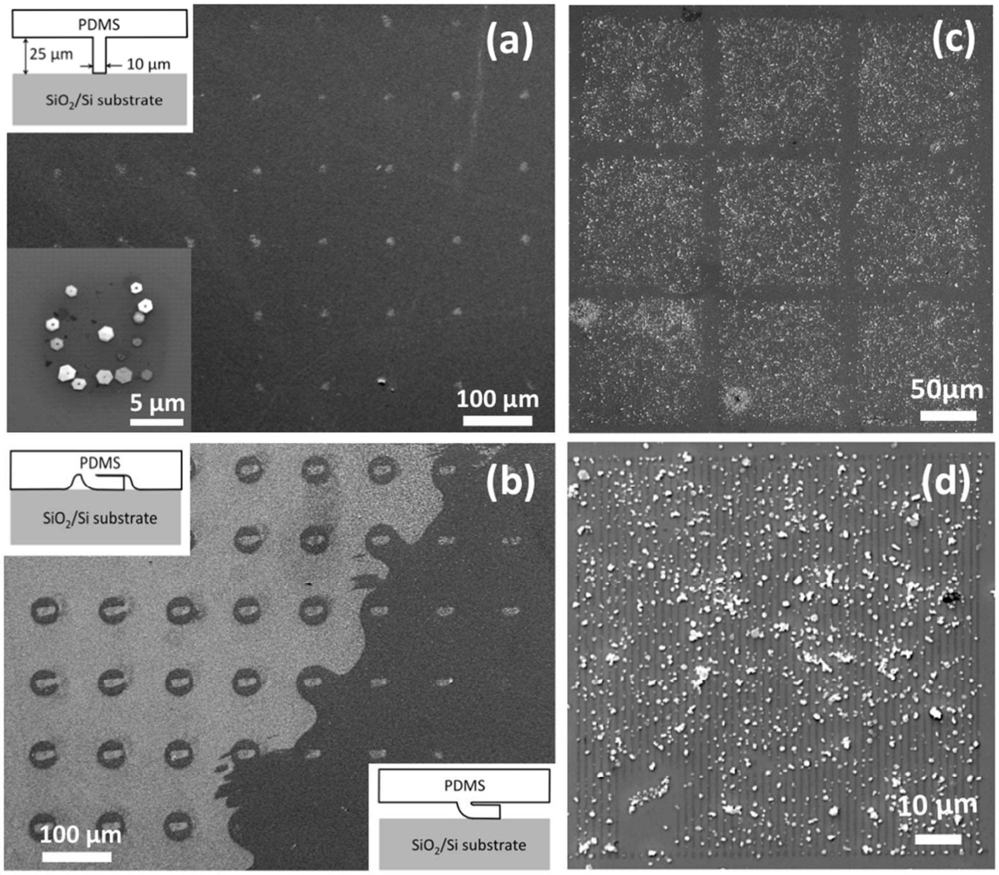

Figure 4
364x317mm (72 x 72 DPI)

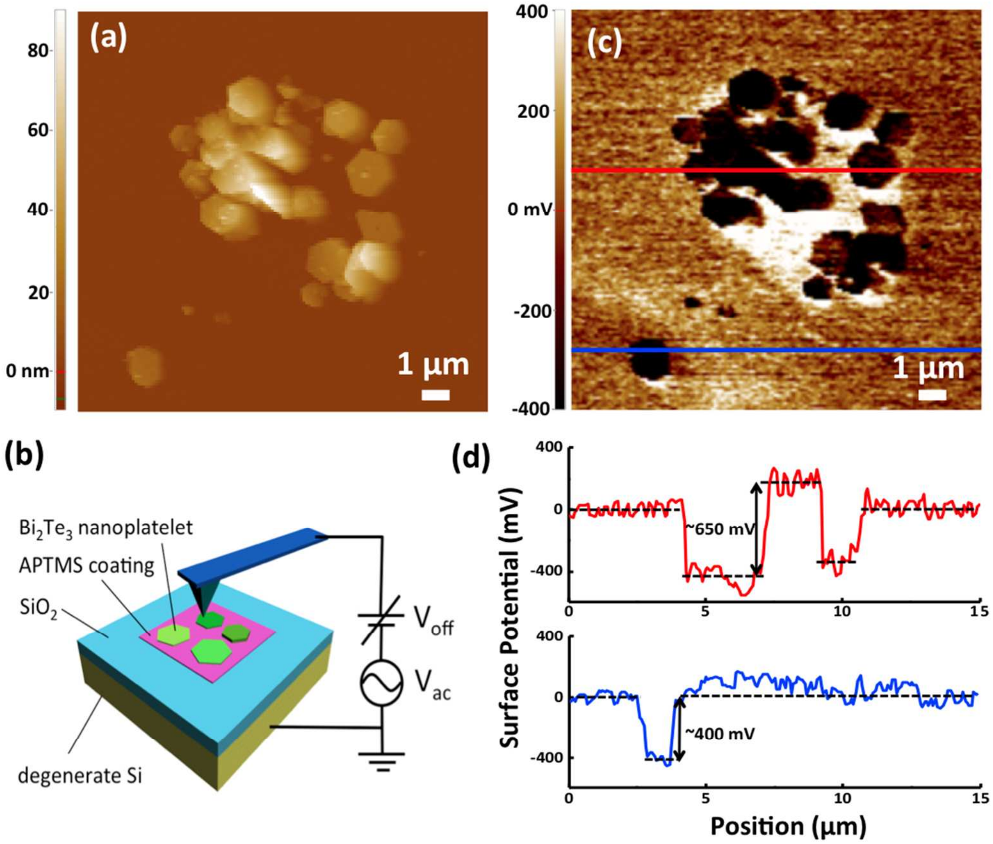

Figure 5
382x321mm (72 x 72 DPI)

Selective Adsorption of Bismuth Telluride Nanoplatelets through Electrostatic Attractions

Lingling Guo,[1,2] Amira Aglan,[1,2] Haiyu Quan,[1,2] Junjie Sun,[2,3] Chaolong Tang,[2,4] Jinhui Song,[2,4] Greg Szulczewski,[2,5] Hung-Ta Wang[1,2,a)]

[1]Department of Chemical and Biological Engineering, University of Alabama, Tuscaloosa, AL 35487, USA.

[2]Center for Materials of Information Technology (MINT Center), University of Alabama, Tuscaloosa, AL 35487, USA.

[3]School of Physics, Shandong University, Jinan, Shandong 250100, China.

[4]Department of Metallurgical and Materials Engineering, University of Alabama, Tuscaloosa, AL 35487, USA.

[5]Department of Chemistry, University of Alabama, Tuscaloosa, AL 35487, USA.

a) Author to whom correspondence should be addressed. Electronic mail: htwang@eng.ua.edu

Text: A controllable adsorption of solution grown Bi_2Te_3 nanoplatelets is demonstrated.

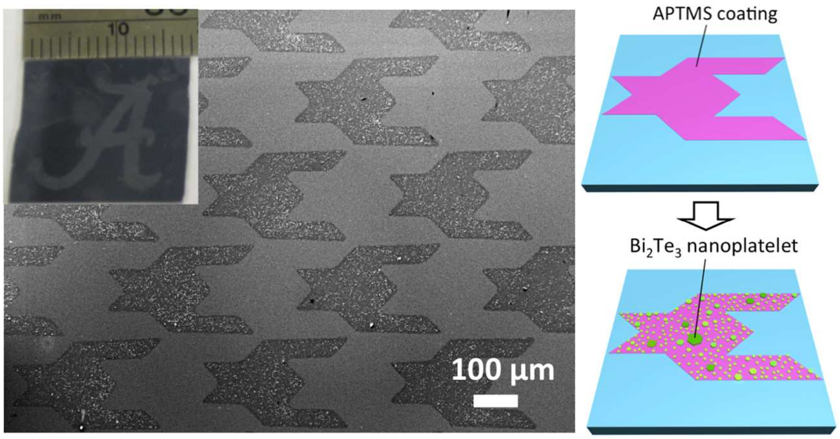

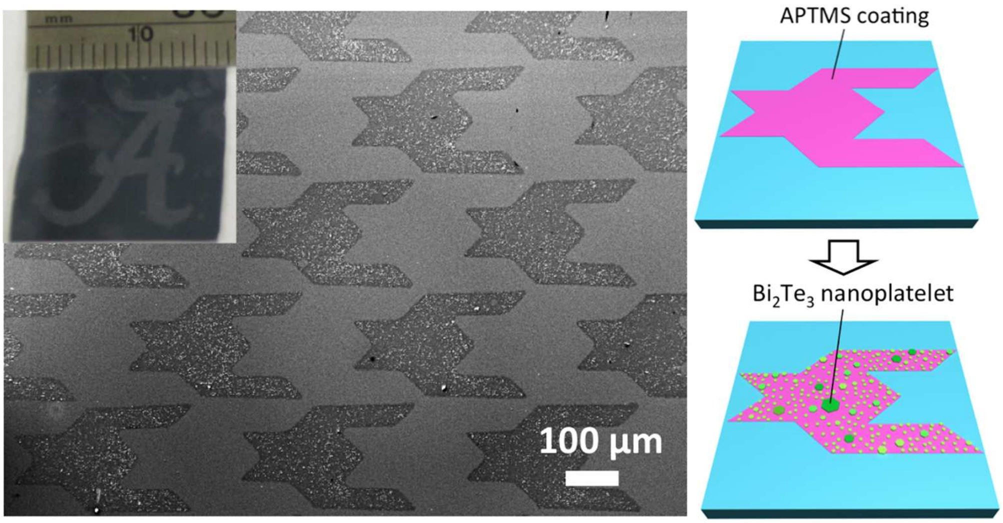

For Graphical Abstract
421x218mm (72 x 72 DPI)

Selective Adsorption of Bismuth Telluride Nanoplatelets through Electrostatic Attractions

Lingling Guo,[1,2] Amira Aglan,[1,2] Haiyu Quan,[1,2] Junjie Sun,[2,3] Chaolong Tang,[2,4] Jinhui Song,[2,4] Greg Szulczewski,[2,5] Hung-Ta Wang[1,2,a)]

[1]Department of Chemical and Biological Engineering, University of Alabama, Tuscaloosa, AL 35487, USA.

[2]Center for Materials of Information Technology (MINT Center), University of Alabama, Tuscaloosa, AL 35487, USA.

[3]School of Physics, Shandong University, Jinan, Shandong 250100, China.

[4]Department of Metallurgical and Materials Engineering, University of Alabama, Tuscaloosa, AL 35487, USA.

[5]Department of Chemistry, University of Alabama, Tuscaloosa, AL 35487, USA.

a) Author to whom correspondence should be addressed. Electronic mail: htwang@eng.ua.edu

Abstract

We demonstrate a facile technique to assemble solution phase-synthesized bismuth telluride (Bi_2Te_3) nanoplatelets into arrays of micropatterns. Aminosilane self-assembled monolayers (SAMs) are printed on silicon dioxide (SiO_2) substrates using microcontact printing (μCP). The SAM printed surfaces are terminated with amine-groups allowing Bi_2Te_3 nanoplatelet selective adsorption owing to an electrostatic attraction. Using Kelvin probe force microscopy, the electrical potential difference between aminosilane SAM and Bi_2Te_3 nanoplatelet surfaces is ~ 650 mV, which is larger than that (~400 mV) between SiO_2 substrate and Bi_2Te_3 nanoplatelet surfaces. The selective adsorption provides an opportunity for integrating solution phase-grown topological insulators toward several device-level applications.

Keywords: Bi_2Te_3 nanoplatelet, microcontact printing, adsorption, topological insulator.

1. Introduction

The V-VI group chalcogenides, including bismuth telluride (Bi_2Te_3), bismuth selenide (Bi_2Se_3), and antimony telluride (Sb_2Te_3), are three-dimensional topological insulators, whose surfaces are covered by the two-dimensional electron gas (2DEG) from the topological surface states.[1-6] The novel topological surface states are induced by a strong spin-orbit coupling, and the spin carriers are protected against time reversal perturbations, e.g., surface defects and impurities, making the 2DEG spin charge transport essentially dissipation-less.[7] Recent advances in topological insulator research have drawn much attention due to its potential application[8] in the next generation electronics,[9, 10] thermoelectrics,[11-14] infrared detectors,[15] and heterogeneous catalysis.[16]

The nontrivial topological surface states of these V-VI group chalcogenides are derived from the unique layered crystal structure. In Bi_2Te_3, five atomic layers in the order of $Te_{(1)}$-Bi-$Te_{(2)}$-Bi-$Te_{(1)}$ form a charge neutral sheet with a thickness of ~1 nm, called a quintuple sheet.[17, 18] Stacking quintuple sheets along the c-axis forms the rhombohedral structure that is in the $D_{3d}^5(R\bar{3}m)$ space group.[19, 20] The adjacent Bi and Te atomic layers in a quintuple sheet are held by covalent forces; in contrast, the bonding between neighboring quintuple layers, i.e., between adjacent $Te_{(1)}$ atomic layers, is a weak van der Waals interaction.[17, 18] Because Bi_2Se_3 has a smaller van der Waals gap than Bi_2Te_3 and Sb_2Te_3, the spin-orbit coupling in Bi_2Se_3 is stronger, and consequently the electronic structures of topological surface states in these V-VI group chalcogenides are also different.[2] Topological surface states in several V-VI group chalcogenides had been revealed by angle-resolved photoemission spectroscopy,[1, 3, 4] scanning-tunneling microscopy,[7] and transport measurements.[5, 6] Currently, the major challenge hampering the novel 2DEG toward practical applications is that the surface spin charge transport is overwhelmed by the ordinary bulk charges. On the other hand, there is a lack of processing techniques suitable for a large scale, device-level integration.

Previously, Bi_2Te_3 and Bi_2Se_3 nanoplatelets were synthesized on mica surfaces by a chemical vapor transport (CVT) method.[21] On the atomically-smooth surfaces, the nanoplatelet growth could be controlled precisely along mica's crystal orientation via the van der Waals epitaxy. Later, arrays of nanoplatelets as flexible infrared transparent electrodes were also demonstrated.[22] Although the van der Waals epitaxy on mica substrates is suitable for selective growth of chalcogenide-based topological insulators, mica substrates are incompatibility with common silicon manufacturing processes, which will limit its use in many applications. In contrast, solvothermal syntheses of Bi_2Te_3 nanoplatelets are facile, and nanoplatelets can be transferred to any substrate. As a result, it is important to develop methods of transferring Bi_2Te_3 nanoplatelets in well-defined positions on silicon substrate to advance the potential applications of these topological insulator nanopletelets.

In this work, we report a practical technique to assemble solution phase-grown Bi_2Te_3 nanoplatelets into micropattern arrays by the microcontact printing (μCP) technique.[23-25] We demonstrate that Bi_2Te_3 nanoplatelets could selectively adsorb onto the surfaces of aminosilane self-assembled monolayers (SAMs) that were printed on silicon oxide (SiO_2) substrates using μCP. We used Kevin probe force microscopy (KPFM) to characterize the surface electrical potentials and measured a ~650 mV potential difference between aminosilane SAMs and Bi_2Te_3 nanoplatelets. The Coulombic interaction between the protonated amine groups and Bi_2Te_3 nanoplatelets enables a robust and scalable method for selectively adsorbing solution phase-grown topological insulator nanoplatelets into micropattern arrays. Such a selective adsorption of topological insulators by aminosilane SAMs also opens the possibilities for topological insulator surface passivation, reduction of ordinary bulk charges, and modification of topological surface states via electrostatic gating. [26, 27]

2. Experimental

Several solvothermal syntheses of Bi_2Te_3 nanoplatelets were previously reported using different precursors and growth conditions in a similar reducing environment.[28-32] Our method is based the approach of Li and co-worker's.[28] The Bi_2Te_3 nanoplatelets were synthesized using the general autoclave reactor (23 ml) from Parr Instrument Company. Bismuth oxide (Bi_2O_3, 99.9995 %), tellurium dioxide (TeO_2, 99.9995 %), ethylene glycol (EG, Reagent Grade), polyvinylpyrrolidone (PVP, average molecule weight 40,000), and sodium hydroxide flakes (NaOH, 98.7 %+) were all purchased from Alfa Aesar. All of the chemicals were used as received without further purification. In a typical synthesis, 0.1865 g of TeO_2, 0.1793 g of Bi_2O_3, 0.3044 g of PVP, and 0.3047 g of NaOH were added into 15 ml of EG. The mixture was stirred vigorously at 90 °C for 30 minutes in order to thoroughly dissolve the chemicals in EG. The precursor solution was sealed in the autoclave reactor, and the solvothermal reaction was carried out in the oven at a temperature of 210 °C for 24 hours. The as-grown nanoplatelets were collected by centrifugation, and cleaned by rinsing alternatively in de-ionized (DI) water at room temperature and 1-methyl-2-pyrrolidone (NMP) at 85 °C for five cycles. It was critical to remove PVP thoroughly to obtain clean Bi_2Te_3 nanoplatelet surfaces for the selective adsorption. The good solubility of PVP in NMP is likely due to the fact that NMP is the pendant group of the polymer, PVP. At an elevated temperature (85 °C), the solubility of PVP in NMP can be further increased. The cleaned Bi_2Te_3 nanoplatelets were characterized by scanning electron microscopy

(SEM, JEOL 7000 FE), X-ray diffraction (XRD, Bruker D8 Discover), atomic force microscopy (AFM, Park XE 70), and transmission electron microscopy (TEM, FEI Tecnai F-20).

The elastic poly(dimethylsiloxane) (PDMS) stamps for the μCP were fabricated by first mixing Sylgard 184 elastomer and curing agent (w/w=10/1) and pouring the mixture over master substrates, which were fabricated by conventional photolithography (Karl Suss MA6) with either SU8-3025 resist or Shipley 1818 resist. After baking at 70 °C for 24 hours, the PDMS was peeled off from the master and cut into a 2×2 cm stamp. To make the μCP ink, (3-aminopropyl)trimethoxysilane (APTMS, 97 % from Sigma-Aldrich) was diluted in DI water to 1 % by volume, sonicated for 3 minutes, and then filtered through a syringe filter (0.2 μm pore size, from VWR). In a standard μCP process, the PDMS stamp was immersed in the filtered 1 % APTMS aqueous solution for 2 minutes and then dried by nitrogen blow. The substrate was an n-type (100) silicon substrate (phosphorus doped, resistivity= 0.001~0.005 ohm•cm) with a thermally-grown dry oxide (thickness~120 nm), which was cleaned by acetone/IPA rinses and oxygen plasma treatment before the μCP. The stamp was brought in contact with SiO_2/Si substrate for 10 to 20 s at 50 °C on the hotplate to ensure the transfer of a single molecular layer of APTMS. The APTMS printed substrate was immediately immersed in the Bi_2Te_3 nanoplatelet-dispersed aqueous solution for 2 to 20 minutes under a mild vortex action. Finally, the substrate was rinsed with DI water and blown dry by a nitrogen gun. The nanoplatelet-dispersed aqueous solution used for the adsorption was prepared by diluting 20 μl highly-concentrated, cleaned nanoplatelet solution in 2 ml DI water, followed by vortex and sonication until a homogeneous nanoplatelet dispersion with a light grey color is obtained. SEM, AFM, and KPFM were used to characterize the APTMS printed and nanoplatelet-adsorbed samples.

3. Results and discussion

Figure 1 presents the structure and chemical characterization of the solution phase-grown Bi_2Te_3 nanoplatelets. As shown by SEM (**Fig. 1(a)** and **(d)**), the Bi_2Te_3 nanoplatelets have a hexagonal morphology owing to the atomic hexagonal packing in the crystal structure. Interestingly, roughly 50 % nanoplatelets have a hole in the center, which may be originated from the growth of a heterostructure of Bi_2Te_3 nanoplatelets skewered by a Te nanowire as observed in the previous reports.[28, 29, 32] It is likely that when Te nanowires are dissolved by NaOH, Bi_2Te_3 nanoplatelets are detached, leaving a hole in the nanoplatelet center. Quantitative analysis of the EDS spectrum (**Fig. 1(b)**) yields the atomic composition of Bi and Te to be 39.55 % and 60.45 %, respectively. The XRD pattern (**Fig. 1(c)**) of the as-synthesized Bi_2Te_3 nanoplatelets can be indexed with the rhombohedral Bi_2Te_3 crystal, and is consistent with the standard data file (PDF card no. 15-0863). In **Fig. 1(e)**, high resolution TEM (HRTEM) and selected area electron diffraction (SAED) performed on the Bi_2Te_3 nanoplatelet show clear lattice fringes and pattern of hexagonally-symmetric spots, respectively. The AFM topographic image (**Fig. 1(f)**) indicates that the lateral size of the nanoplatelets is roughly in the range of 500 nm to 3 μm, and the thickness is about 10 nm to 100 nm. Collectively, the HRTEM, SAED, and XRD data indicate that our solvothermal synthesis produced highly crystallized Bi_2Te_3 nanoplatelets, which is consistent with the report of Li *et al.*[28]

We note that cleaned Bi_2Te_3 nanoplatelets have a low affinity to SiO_2 surfaces using either drop casting or dip coating. A low nanoplatelet coating density was consistently obtained, and it showed trivial dependences with the nanoplatelet dispersion concentration, transferring (adsorption) time, and SiO_2 substrate hydrophobic/hydrophilic property. When a high concentration Bi_2Te_3 nanoplatelet dispersion was applied, nanoplatelets tended to aggregate to form clusters in local regions (i.e., nanoplatelets randomly pile up), and most areas were still covered with a low density of nanoplatelets. The low affinity between the Bi_2Te_3 nanoplatelets and SiO_2 surfaces reveals a great challenge for assembling nanoplatelets toward practical applications.

To provide a feasible solution, we printed SAMs of APTMS, where were expected to have a strong affinity to Bi_2Te_3 nanoplatelet surface. **Figure 2** demonstrates the selective adsorption of Bi_2Te_3 nanoplatelets using the logo of the University of Alabama. The area of the logo “A” consists of an array of APTMS printed houndstooth patterns, and Bi_2Te_3 nanoplatelets were adsorbed mainly onto the APTMS printed regions. Interestingly, nanoplatelet aggregation (or stacking) frequently observed before was greatly reduced. More importantly, and the selective adsorption can be consistently obtained, and the nanoplatelet coating density could be tuned by varying the adsorption time (shown in the Supplementary Information). This general μCP of SAMs of aminosilane was first reported for the selective adsorption of negatively-charged nanomaterials by Zhang *et al.*[23] Despite a ~50 % self-catalyzed hydrolysis of (3-aminopropyl)triethoxysilane (APTES) in aqueous solutions at room temperature,[33, 34] Zhang *et al.* demonstrated that using hydrophobic PDMS stamps with aqueous APTES inks could still print APTES monolayers. Although the printed APTES did not entirely form SAMs as noted in their work, the amine group terminated surfaces were very effective for the selective adsorption of citrate-coated Au nanoparticles and negatively-charged graphene oxide nanosheets. This is believed that due to an electrostatic interaction, the negatively-charged nanoparticles/nanosheets are attracted by the positively-charged, protonated amine group surfaces, resulting a controllable adsorption.[23, 35] We demonstrate that this general μCP technique is very suitable to selectively adsorb topological insulator nanoplatelets.

Although the Bi_2Te_3 nanoplatelet selective adsorption could originate from the similar electrostatic interaction, we observed that Bi_2Te_3 nanoplatelets had a distinct adsorption behavior than Au nanoparticles.[23, 35] By immersing APTMS printed substrates in Bi_2Te_3 nanoplatelet dispersed aqueous solutions, a low density of Bi_2Te_3 nanoplatelet adsorption with a poor selectivity was obtained surprisingly. In contrast, when a mild vortex was applied during the adsorption of Bi_2Te_3 nanoplatelets and while other μCP conditions were kept the same, the adsorption density was greatly increased and the adsorption selectivity was also improved. Owing to the hexagonally-shaped nanoplatelet morphology, nanoplatelet adsorption to a planar surface is limited to the top or bottom nanoplatelet surfaces. When nanoplatelets were dispersed in an unstirred aqueous solution, the nanoplatelets were observed (in an optical microscope) to undergo a flipping-type motion. Consequently, dispersed nanoplatelets had a reduced chance for the top or bottom nanoplatelet surfaces well contacting with APTMS printed surfaces to form an adsorption. This is different to Au nanoparticle adsorption, as when any points of a sphere surface in contact with a planar surface, an adsorption would easily occur. With a mild vortexing-action, the Bi_2Te_3 nanoplatelets in the dispersed aqueous solution were constantly colliding with the substrate surface, so that the chance for a face-to-face contact between nanoplatelet top/bottom surfaces and APTMS surfaces was highly increased. At the same time, when nanoplatelets were in contact with bare SiO_2 surfaces, the low affinity might not be strong enough to retain the adsorption, and nanoplatelets could be carried away by the vortex.

In order to obtain a stronger electrostatic interaction for Bi_2Te_3 nanoplatelet adsorption, we used *in situ* annealing during the μCP at a temperature of 50 °C. As shown in **Figure 3**, the thickness of the APTMS coating clearly increased from 4 - 20 Å (μCP at room temperature) to 8 - 20 Å (μCP at 50 °C), and the density of APTMS also improved with the *in situ* annealing. It is clear that there are still APTMS particles with a height of ~2 nm formed both with and without an *in situ* annealing, which is likely from the condensation in the aqueous ink.[23] Excluding those APTMS particles, it is shown that the average APTMS height is 4 Å without *in situ* annealing, and 8 Å with the *in situ* annealing. This implies APTMS formed sub-monolayers at room temperature, while a better packing was preferred at 50 °C to produce a monolayer.[33] It was previously reported that in toluene (i.e., no hydrolysis effect), *in situ* annealing at 70 °C could improve the packing quality of APTES on SiO_2 surfaces.[36] This is explained by the fact that the *in situ* annealing facilitates the formation of horizontal Si-O-Si bonds between adjacent APTES molecules, and the effect is an increased packing density. We suspect that the *in situ* annealing during μCP also improved the APTMS packing quality via the similar mechanism (i.e., formation of horizontal Si-O-Si bonds between APTMS). As the amine group density was increased from a closely packed APTMS SAM, Bi_2Te_3 nanoplatelet adsorption selectivity was repeatedly obtained.

We further present the selective adsorption of Bi_2Te_3 nanoplatelets using stamps of either 10×10 μm square array (as shown in **Fig. 4(a)** and **(b)**) or 1×100 μm line array (as shown in **Fig. 4(c)** and **(d)**). Due to the softness of the PDMS and the dimension of the square pillar array (shown in **Fig. 4(a)** inset), the PDMS stamps could sag and/or collapse to cause different μCP patterns.[25] As shown in **Fig. 4(a)** and **(b)**, the selective adsorption of Bi_2Te_3 nanoplatelets reveals the three μCP patterns, induced by the PDMS stamp (1) contacted normally, (2) collapsed plus sagged, and (3) collapsed only, respectively. This result shows that the selective adsorption could be robustly obtained on a 10×10 μm APTMS printed surface. To further test the robustness of the selective adsorption, we used PDMS stamps with the 1×100 μm line array. **Fig. 4(c)** and **(d)** show that Bi_2Te_3 nanoplatelets mainly adsorb onto the APTMS printed lines. Indeed, there are still un-wanted nanoplatelets adsorbed on the bare SiO_2 surface due to the affinity between Bi_2Te_3 nanoplatelets and SiO_2 surfaces. Nevertheless, it should be noted that the line width is comparable with the nanoplatelet lateral size, suggesting that under a vortex motion, the electrostatic interaction between Bi_2Te_3 nanoplatelets and APTMS printed surfaces is quite reliable to produce the nanoplatelet selective adsorption.

To understand the electrostatic interaction between APTMS monolayer and the Bi_2Te_3 nanoplatelet surfaces, we examined the adsorbed Bi_2Te_3 nanoplatelets by KPFM. As shown in **Figure 5**, the surface electrical potential difference between Bi_2Te_3 surfaces and APTMS printed surfaces is about 650 mV. In comparison, the surface electrical potential difference between Bi_2Te_3 surfaces and SiO_2 surfaces is ~400 mV, which is comparable to the report of Hao *et al*.[37] It should be noted that the surface electrical potentials are measured under ambient conditions and not in an aqueous environment. With the existence of electrical double layers formed on the charged surfaces in an aqueous solution,[38] the electrostatic forces experienced by the Bi_2Te_3 nanoplatelets during the adsorption should be quite different from what was measured by KPFM. Nevertheless, our data has implied that in an aqueous solution, the electrostatic attraction force between APTMS surfaces and Bi_2Te_3 nanoplatelets was stronger than that between bare SiO_2 surfaces and Bi_2Te_3 nanoplatelets, allowing the selective adsorption of Bi_2Te_3 nanoplatelets.

4. Conclusion

In summary, we have presented a practical method to selectively adsorb solution phase grown topological insulator nanoplatelets onto APTMS printed surfaces via μCP. Owing to the specific nanoplatelet morphology, a vortex treatment during the adsorption facilitates the nanoplatelet adsorption and simultaneously improves the adsorption selectivity. We also show that APTMS monolayer packing can be improved by an *in situ* annealing at 50 °C during μCP, which further enhances the nanoplatelet adsorption. The electrical potential difference, measured by KPFM, between aminosilane SAMs and Bi_2Te_3 nanoplatelet surfaces is larger than that between SiO_2 and Bi_2Te_3 surfaces. We attribute the selective adsorption of Bi_2Te_3 nanoplatelets to this electrostatic interaction. Such a general adsorption of negatively-charged topological insulators is suitable for a large-scale assembly and device level fabrication.

Acknowledgements

This work at the University of Alabama (UA) is supported by the UA start-up fund and the 2012 UA Research Grants Committee (RGC) award. L. Guo would like to acknowledge the support from UA MINT Graduate Student Scholarship. A. Aglan would like to acknowledge the support from the National Science Foundation Research Experiences for Undergraduates Program (EEC-1005191; National Academy Grand Challenges), and the UA Emerging Scholar program. J. Sun would like to acknowledge the 2013 Summer Internship Program (SIP) hosted by the UA MINT Center. Authors greatly acknowledge the instrumental supports from UA Microfabrication Facility (MFF), UA Central Analytical Facility (CAF), and the UA MINT Center.

Figure Captions

Figure 1. **(a)** SEM image of the cleaned Bi_2Te_3 nanoplatelets. Inset: photograph of the vials with as-grown and cleaned nanoplatelet solution. **(b)** EDS and **(c)** XRD of cleaned Bi_2Te_3 nanoplatelets. **(d)** High magnification SEM image of the Bi_2Te_3 nanoplatelet. **(e)** TEM image of the Bi_2Te_3 nanoplatelet. Insets are HRTEM and SAED, respectively. **(f)** AFM topographic image of the Bi_2Te_3 nanoplatelets with their thicknesses labeled accordingly.

Figure 2. **(a)** Photograph of the silicon chip with selective adsorption of Bi_2Te_3 nanoplatelets to reveal the logo of "A," in which the area consists of a houndstooth array. **(b)** SEM image of Bi_2Te_3 nanoplatelets selective adsorption onto the houndstooth array that is in a local region of the logo "A" shown in (a). **(c)** SEM image of a houndstooth pattern with APTMS coating via µCP, as illustrated by the cartoon. The dark region is the APTMS coating. **(d)** SEM image of a houndstooth pattern with the Bi_2Te_3 nanoplatelet adsorption, as illustrated by the cartoon. The white dots are nanoplatelets, as magnified in the SEM inset.

Figure 3. AFM topographic images of the APTMS coating prepared by µCP for 10s **(a)** without, and **(b)** with 50 °C *in situ* annealing, respectively. The PDMS stamp contains an array of lines (line width × length = 1×100 µm). The topographic profiles (the green lines) are plotted and the scale bar is 1 nm.

Figure 4. **(a)** SEM image of the selective adsorption of Bi_2Te_3 nanoplatelets using an array of 10×10 µm squares. The magnified SEM image (inset) shows that the nanoplatelets adsorbed onto the APTMS printed, 10×10 µm square. The square pattern was obtained with the stamp in a

normal contact, as illustrated in the inset. **(b)** SEM image of the selective adsorption of Bi_2Te_3 nanoplatelets reveals the two patterns printed with the stamp sagged plus collapsed (left region), and collapsed only (right region), respectively, as illustrated in the insets. Note that these two patterns and the square pattern shown in (a) were obtained from the same substrate. **(c)** SEM image of the selective adsorption using an array of 1×100 μm lines. **(d)** Magnified SEM image shows that Bi_2Te_3 nanoplatelets adsorbed mainly onto the APTMS printed lines.

Figure 5. (a) AFM topographic image of the Bi_2Te_3 nanoplatelets adsorbed in the APTMS printed, 10×10 μm square region. **(b)** Schematic of the electrical configuration for the Kevin probe force microscope measurement. **(c)** The electrical potential image scanned in the same area as shown in (a). Note that all nanoplatelets are on the APTMS printed region, except the nanoplatelet in the left/bottom corner that is on the bare SiO_2 surface. **(d)** The surface electrical potential profiles corresponding to the red and blue line marked in (c) are plotted, respectively.

References

1. Y. L. Chen, J. G. Analytis, J. H. Chu, Z. K. Liu, S. K. Mo, X. L. Qi, H. J. Zhang, D. H. Lu, X. Dai, Z. Fang, S. C. Zhang, I. R. Fisher, Z. Hussain and Z. X. Shen, *Science*, 2009, **325**, 178-181.
2. H. J. Zhang, C. X. Liu, X. L. Qi, X. Dai, Z. Fang and S. C. Zhang, *Nature Physics*, 2009, **5**, 438-442.
3. D. Hsieh, Y. Xia, D. Qian, L. Wray, J. H. Dil, F. Meier, J. Osterwalder, L. Patthey, J. G. Checkelsky, N. P. Ong, A. V. Fedorov, H. Lin, A. Bansil, D. Grauer, Y. S. Hor, R. J. Cava and M. Z. Hasan, *Nature*, 2009, **460**, 1101-1105.
4. Y. Xia, D. Qian, D. Hsieh, L. Wray, A. Pal, H. Lin, A. Bansil, D. Grauer, Y. S. Hor, R. J. Cava and M. Z. Hasan, *Nature Physics*, 2009, **5**, 398-402.
5. H. L. Peng, K. J. Lai, D. S. Kong, S. Meister, Y. L. Chen, X. L. Qi, S. C. Zhang, Z. X. Shen and Y. Cui, *Nature Materials*, 2010, **9**, 225-229.
6. D.-X. Qu, Y. S. Hor, J. Xiong, R. J. Cava and N. P. Ong, *Science*, 2010, **329**, 821-824.
7. P. Roushan, J. Seo, C. V. Parker, Y. S. Hor, D. Hsieh, D. Qian, A. Richardella, M. Z. Hasan, R. J. Cava and A. Yazdani, *Nature*, 2009, **460**, 1106-1109.
8. D. Kong and Y. Cui, *Nature Chemistry*, 2011, **3**, 845-849.
9. I. Garate and M. Franz, *Physical Review Letters*, 2010, **104**, 146802.
10. H. Steinberg, D. R. Gardner, Y. S. Lee and P. Jarillo-Herrero, *Nano Letters*, 2010, **10**, 5036.
11. A. Soni, Y. Zhao, L. Yu, K. A. Khor, M. S. Dresselhaus and Q. Xiong, *Nano Letters*, 2012.

12. R. J. Mehta, Y. Zhang, C. Karthik, B. Singh, R. W. Siegel, T. Borca-Tasciuc and G. Ramanath, *Nature Materials*, 2012, **11**, 233-240.
13. M. T. Pettes, J. Maassen, I. Jo, M. S. Lundstrom and L. Shi, *Nano Letters*, 2013, **13**, 5316-5322.
14. P. Puneet, R. Podila, M. Karakaya, S. Zhu, J. He, T. M. Tritt, M. S. Dresselhaus and A. M. Rao, *Scientific Reports*, 2013, **3**.
15. X. Zhang, J. Wang and S.-C. Zhang, *Physical Review B*, 2010, **82**, 245107.
16. H. Chen, W. Zhu, D. Xiao and Z. Zhang, *Physical Review Letters*, 2011, **107**, 056804.
17. D. S. Kong, W. H. Dang, J. J. Cha, H. Li, S. Meister, H. L. Peng, Z. F. Liu and Y. Cui, *Nano Letters*, 2010, **10**, 2245-2250.
18. D. Teweldebrhan, V. Goyal and A. A. Balandin, *Nano Letters*, 2010, **10**, 1209-1218.
19. Y. Feutelais, B. Legendre, N. Rodier and V. Agafonov, *Materials Research Bulletin*, 1993, **28**, 591-596.
20. W. Richter and C. R. Becker, *Physica Status Solidi (b)*, 1977, **84**, 619-628.
21. H. Li, J. Cao, W. Zheng, Y. Chen, D. Wu, W. Dang, K. Wang, H. Peng and Z. Liu, *Journal of the American Chemical Society*, 2012, **134**, 6132-6135.
22. H. Peng, W. Dang, J. Cao, Y. Chen, D. Wu, W. Zheng, H. Li, Z.-X. Shen and Z. Liu, *Nature Chemistry*, 2012, **4**, 281-286.
23. H. Li, J. Zhang, X. Zhou, G. Lu, Z. Yin, G. Li, T. Wu, F. Boey, S. S. Venkatraman and H. Zhang, *Langmuir*, 2009, **26**, 5603-5609.
24. L. Libioulle, A. Bietsch, H. Schmid, B. Michel and E. Delamarche, *Langmuir*, 1998, **15**, 300-304.
25. D. Qin, Y. Xia and G. M. Whitesides, *Nature Protocols*, 2010, **5**, 491-502.

26. S. S. Hong, J. J. Cha, D. Kong and Y. Cui, *Nature Communications*, 2012, **3**, 757.
27. D. Kim, S. Cho, N. P. Butch, P. Syers, K. Kirshenbaum, S. Adam, J. Paglione and M. S. Fuhrer, *Nature Physics*, 2012, **8**, 459-463.
28. G. Q. Zhang, W. Wang, X. L. Lu and X. G. Li, *Crystal Growth & Design*, 2009, **9**, 145-150.
29. W. Lu, Y. Ding, Y. Chen, Z. L. Wang and J. Fang, *Journal of the American Chemical Society*, 2005, **127**, 10112-10116.
30. W. Wang, B. Poudel, J. Yang, D. Z. Wang and Z. F. Ren, *Journal of the American Chemical Society*, 2005, **127**, 13792-13793.
31. J. Zhang, Z. P. Peng, A. Soni, Y. Y. Zhao, Y. Xiong, B. Peng, J. B. Wang, M. S. Dresselhaus and Q. H. Xiong, *Nano Letters*, 2011, **11**, 2407-2414.
32. H. Fang, T. Feng, H. Yang, X. Ruan and Y. Wu, *Nano Letters*, 2013, **13**, 2058-2063.
33. M. Zhu, M. Z. Lerum and W. Chen, *Langmuir*, 2011, **28**, 416-423.
34. E. T. Vandenberg, L. Bertilsson, B. Liedberg, K. Uvdal, R. Erlandsson, H. Elwing and I. Lundström, *Journal of Colloid and Interface Science*, 1991, **147**, 103-118.
35. J. Zheng, Z. Zhu, H. Chen and Z. Liu, *Langmuir*, 2000, **16**, 4409-4412.
36. R. M. Pasternack, S. Rivillon Amy and Y. J. Chabal, *Langmuir*, 2008, **24**, 12963-12971.
37. G. Hao, X. Qi, L. Yang, Y. Liu, J. Li, L. Ren, F. Sun and J. Zhong, *AIP Advances*, 2012, **2**, 012114-012118.
38. J. Israelachvili, *Intermolecular and Surface Forces*, Third Edn., Academic Press, London, 2011.